Journal of Hydrology (2008) **358**, 70–83

available at www.sciencedirect.com

ScienceDirect

journal homepage: www.elsevier.com/locate/jhydrol

Uncertainty of the impact of climate change on the hydrology of a nordic watershed

Marie Minville *, François Brissette, Robert Leconte

Department of Construction Engineering, École de Technologie Supérieure, Université du Québec, 1100 Notre-Dame Ouest, Montréal, Quebec, Canada H3C 1K3

Received 21 August 2007; received in revised form 22 May 2008; accepted 22 May 2008

KEYWORDS
Climate change;
Hydrology;
Uncertainty;
Variability;
Stream flow;
Snow

Summary The impact of climate change on the hydrology of the Chute-du-Diable watershed (Quebec, Canada) is studied by comparing statistics on current and projected future discharge resulting from a wide range of climate change scenarios. The use of 10 equally weighted climate projections from a combination of 5 general circulation models (GCMs) and 2 greenhouse gas emission scenarios (GHGES) allows for the definition of an uncertainty envelope of future hydrologic variables. GCM data is downscaled using the change factor approach for 30-year time slices centered around years 2020, 2050 and 2080.

To estimate natural variability, synthetic time series are then computed for each horizon and for each climate change scenario, using a stochastic weather generator (30 series of 30 years), and are entered into a hydrology model. Future hydrological regimes are then compared to the control period (1961–1990) using the annual and seasonal mean discharge, peak discharge and timing of peak discharge criteria.

Results indicate a 1–14 °C increase in seasonal temperature and a −9 to +55% change in seasonal precipitation. The largest increases in both temperature and precipitation are observed in the winter and spring seasons. The main hydrologic impact observed is a spring flood appearing 1–5 weeks earlier than usual and a modification of its amplitude from −40 to +25%. Most scenarios suggest increases in the winter, spring and fall discharge, whereas summer is expected to see a decrease in discharge. While there is still a large scatter in projected values, the uncertainty analysis projects a better view of the most probable future hydrologic behaviour of the watershed.

Of all sources of uncertainty considered in this study, the largest comes from the choice of a GCM. Accordingly, all impact studies based on results from only one GCM should be interpreted with caution.

* Corresponding author. Tel.: +1 514 282 6464x285; fax: +1 514 396 8584.
E-mail addresses: marie.minville@etsmtl.ca (M. Minville), francois.brissette@etsmtl.ca (F. Brissette), robert.leconte@etsmtl.ca (R. Leconte).

0022-1694/$ - see front matter © 2008 Elsevier B.V. All rights reserved.
doi:10.1016/j.jhydrol.2008.05.033

Nomenclature

$P_{fut,j,h}$	future precipitation at day j and horizon h	$T_{obs,j}$	observed historical time series of temperature at day j
$P_{obs,j}$	observed historical time series of precipitation at day j	$\overline{T}_{fut,m,h}$	simulated future temperature at month m and horizon h
$\overline{P}_{fut,m,h}$	simulated future precipitation at month m and horizon h	$T_{cont,m}$	simulated actual temperature at month m
$P_{cont,m}$	simulated actual precipitation at month m	ω_n	weight of the nth grid point
$T_{fut,j,h}$	future temperature at day j and horizon h		

Introduction

In the future, water is the resource that will be most severely affected by climate change (Environement Canada, 2004, 1996; Srikanthan and McMahon, 2001; Xu and Singh, 2004). Several studies (Whitfield and Cannon (2000); Muzik (2001); Risbey and Entekhabi (1996); among others) have shown that small perturbations in precipitation frequency and/or quantity can result in significant impacts on the mean annual discharge. Moreover, Christensen et al., 2004 mention that modest changes in natural inflows result in larger changes in reservoir storage. Any changes in the hydrologic cycle will affect energy production and flood control measures (Xu and Singh, 2004) to such an extent that water management adaptation measures will very likely be brought in.

Whitfield and Cannon (2000) have analyzed recent hydrologic trends in Canada (1976—1995), and have observed that several regions display hydrographs with an early spring flood and increased winter mean discharge as well as smaller summer flows. Regonda et al. (2005) did a similar analysis in the United Sates on North West basins and observed an advancing trend in the timing of peak spring flows, which he attributed to climate change. An increase in winter precipitations was also observed. This precipitation increase did not however translate into higher spring discharges, suggesting that the precipitation trend was offset by higher temperatures and increased winter seasonal melt and more liquid precipitation.

Similarly, the IPCC (2001) states that over the course of this century, North-American river inflows will rise in the winter season, while decreases will be observed in the summer. In the Canadian province of Quebec, the impact of such changes on hydropower is critical. In Northern Quebec, annual reservoir inflows are expected to rise (Ouranos, 2004). This is generally considered to be a positive impact, although it may not necessarily result in increased hydropower production. On the other hand, the projected increase in extreme rainfall events in the southern areas, where most of Quebec's population is concentrated, will likely increase damage due to floods. Water management and design practices will face new challenges which will require a better quantitative understanding of potential changes; this understanding of the impacts of climate change is complicated by several sources of uncertainty linked to climate change. The uncertainty depends on both climate data and simulated hydrologic regimes (Prudhomme et al., 2003). Climatic uncertainty is linked to greenhouse gas emission scenarios (GHGES) and especially to general circulation models (GCMs), whose representation of topography and climate processes is imperfect, in large parts due to computational limitations. The future climate uncertainty has recently been introduced into hydrology impact studies by using more than one climate projection obtained from the combination of GCM and GHGES. Recently Merritt et al. (2006) and Vicuna et al. (2007) used 3 GCMs and 2 GHGES. Maurer (2007), also for an hydrology impact study used 11 GCM and 2 GHGES, and although not all of the possible combinations were used, this points to a tendency in using as many GCM and GHGES as possible to better encompass the uncertainty linked with climate projections.

Downscaling methods also add uncertainty to climate data due to the limitations that are inherent in each technique. Hydrologic uncertainty results from the transferability of hydrological models to a future climate, and particularly with respect to model calibration. Considering all these sources of uncertainty, future hydrologic conditions can only be described by taking into account as much of this uncertainty as possible. As such, a precise deterministic prediction is not possible.

The main objective of this work is to quantify the impacts of climate change on the Chute-du-Diable watershed, while outlining the uncertainty linked to climate data by considering data from several GCMs and GHGES. This is the first part of a larger project that aims to propose adaptation measures for water management practices over the watershed.

The paper first presents the main characteristics of the watershed. Climate data is then presented, followed by details on how climate change projections were constructed. The paper concludes with a presentation of results and a discussion.

Study area and historical data

The Chute-du-Diable watershed is located close to the geographical center of the province of Quebec (Fig. 1) and is part of the Peribonka River watershed. It has a surface area of 9700 km^2, with an elevation of between 100 and 700 m. It is sparsely populated, and mostly forested. The watershed is used mainly for hydropower production and logging. The average annual rainfall in the area is 962 mm and the basin's annual average temperature is -1 °C. Snowfall accounts for over 36% of the mean annual precipitation. Daily area-averaged meterological data was derived from a network of 6 gauges distributed throughout the catchment averaged over 26 years of historical data. River flows are regulated by two

Figure 1 Location map of Chute-du-Diable watershed with location of hydrometeorological stations (black circles).

upstream reservoirs. Natural (de-regulated) inflows used in this study were obtained from the Énergie Électrique Company, a division of Rio Tinto Alcan, a world-leading aluminum producer. Snow plays a crucial role in the watershed management, with 35% of the total yearly discharge occurring during the spring flood. The mean annual inflow of the Chute-du-Diable watershed is 212 m^3/s.

This watershed was chosen since it contains 3 hydropower plants managed by a division of Alcan Inc. The work outlined in this paper is part of a larger project aimed at the evaluation of potential impacts of climate change on water management practices and hydropower production over the Peribonka River watershed.

Hydrological model description and calibration

Hydrological model: HSAMI

Hydrological modelling was performed with the HSAMI software model (Bisson and Roberge, 1983; Fortin, 2000), which was developed by Hydro-Québec, and as been routinely used in forecasting natural inflows for over 20 years. HSAMI is actually used in Quebec for daily forecasting of natural inflows on 84 watersheds with surface areas ranging from 160 km^2 to 69195 km^2. Verticals flows are simulated with 4 interconnected linear reservoirs (snow on the ground, surface water, unsaturated and saturated zones). The model takes into account snow accumulation, snowmelt, soil freezing/thawing and evapotranspiration. Water is transferred at the basin outlet through surface runoff, interflow and baseflow (see Fig. 2). For each time step, the model goes through the following steps:

1. Estimation of potential evapotranspiration.
2. Computation of net precipitation on reservoirs.
3. Simulation of interception and accumulation of rainfall and snow, interactions between rainfall and snow, snowpack freezing/thawing and aging.
4. Separation of available surface water between infiltration and runoff.
5. Simulation of vertical water movement (infiltration, interflow, evapotranspiration and movement between the saturated and unsaturated zones).
6. Simulation of horizontal flows toward the outlet.
7. Computation of natural inflows or water discharge at the outlet.

HSAMI is a 23-parameter, lumped, conceptual, rainfall-runoff model. Two parameters account for evapotranspiration, 6 for snowmelt, 10 for vertical water movement, and 5

for horizontal water movement. Model calibration is done automatically using the shuffled complex evolution optimisation method (Duan, 2003).

The basin-averaged required daily input data for the model is: minimum and maximum temperatures, liquid and solid precipitations. Sunshine hours and snow on ground are optional inputs. A natural inflows or discharge time series is also needed for proper calibration/validation.

Calibration/validation of hydrological model

As mentioned previously, since HSAMI is a lumped model, the initial step consisted in preparing basin-averaged data input. Six years were used for calibration (1978—1983), and 20 years for validation (1984—2003). The more recent years were favoured because they provide calibration/validation for the warmest years on record. The uncertainty linked to model calibration in a future climate was not considered in this study. The optimal combination of parameters was chosen based on the Nash-Sutcliffe criteria for both calibration and validation runs. The chosen set of parameters yielded values of the Nash-Sutcliffe criteria of 0.92 for calibration and 0.89 for validation.

Fig. 3 presents the observed and modeled averaged hydrographs for the 1978—2003 time period. The model behaves well most of the year, with the exception of summer, when the modeled discharge is overestimated.

Climate change projections

Methodology

Climate change projections used in this project are constructed in three steps. First, climate projections from GCMs and GHGES are selected, and then climate data is downscaled to allow its use at the basin scale. Finally, several synthetic time series of downscaled climate data are stochastically generated to take into account the natural year-to-year climate variability.

General circulation models (GCMs) and greenhouse gas emission scenarios (GHGES)

The climate projections (Table 1) selected are obtained from 5 GCMs and 2 GHGES (Nakicenovic et al., 2000). The chosen GCMs are the United Kingdom climate model (HadCM3), the European climate model (ECHAM4), the Australian model (CSIRO), the Japanese climate model (CCSRNIES) and the Canadian climate model (CGCM3).

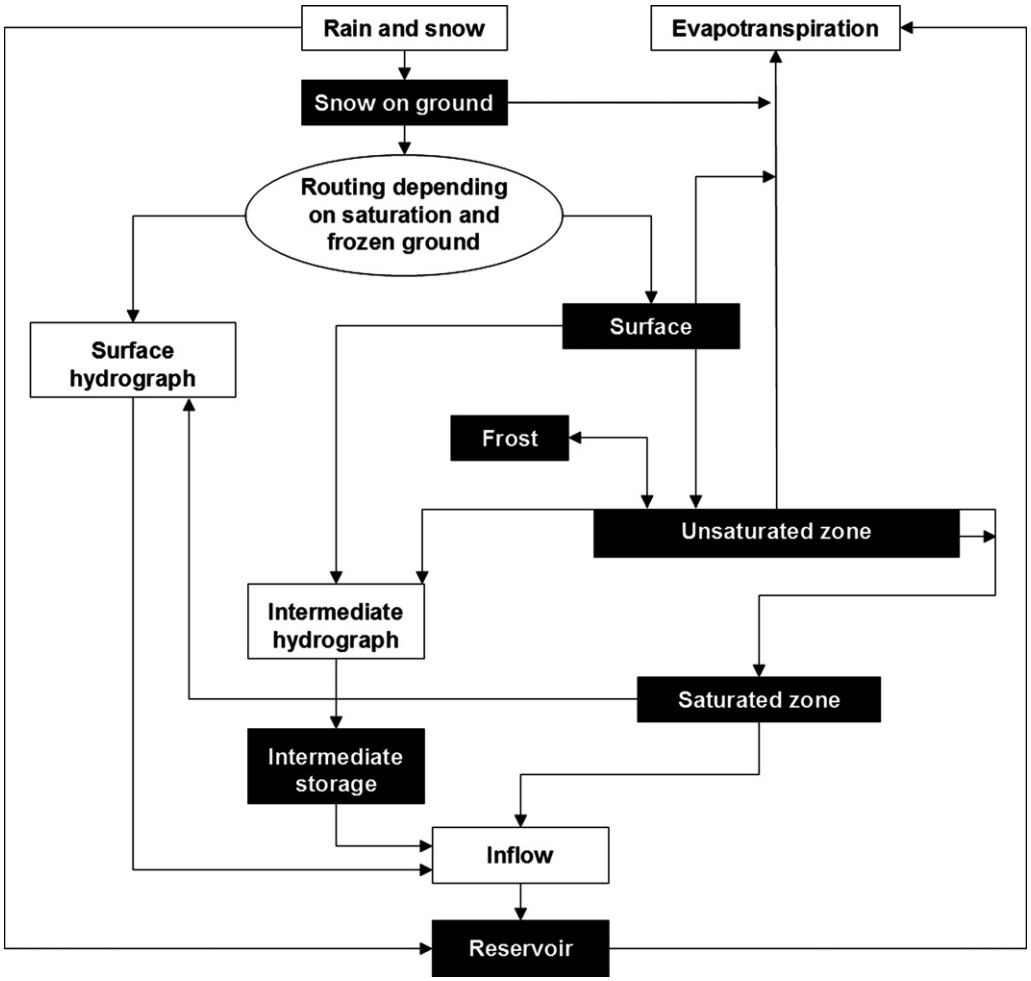

Figure 2 Flow chart of the HSAMI model.

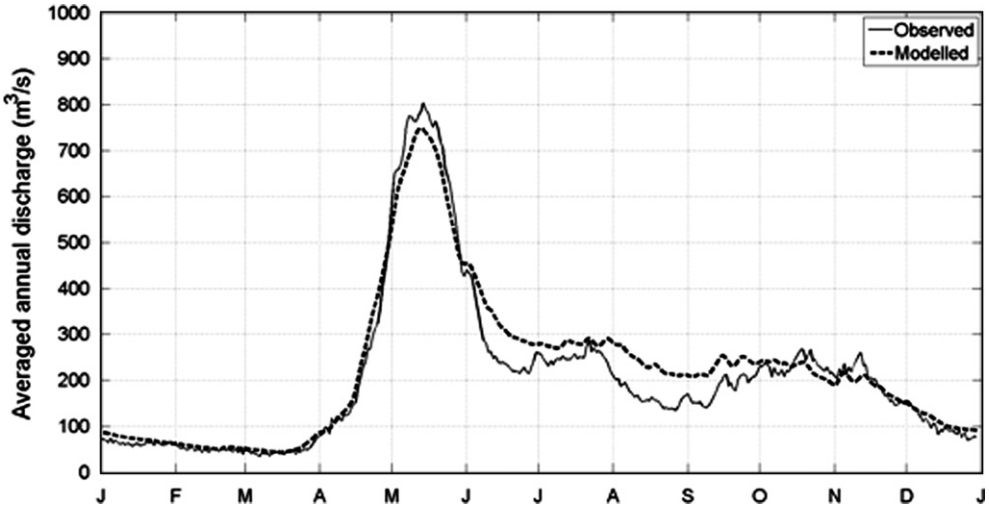

Figure 3 Observed and modelled averaged hydrographs for the 1978—2003 time period for the Chute-du-Diable watershed.

Table 1 Climate projections used

	A2	B1	B2
HadCM3	√		√
ECHAM4	√		√
CSIRO	√		√
CCSRNIES	√		√
CGCM3	√	√	

These models have all been used in the atmospheric model inter-comparison project (Boer, 2004), with the exception of the third version of the Canadian climate model (CGCM3), which is more recent. All GCMs are able to simulate the climate and its variability, even though the atmospheric processes are not all perfectly represented due to the coarse computational grid of the models, and the still limited understanding of some processes (Boer, 2004). For the CGCM3 model, since results from the B2 scenario were not available, the B1 scenario (a more optimistic scenario) was chosen instead. Implications of this choice will be examined in the discussion section.

Bias correction

Bias correction is needed to remove bias between model and observations over the study region. While some climate data is well represented by GCMs, certain other outputs (including precipitation) are often not well reproduced (Roy et al., 2001). The bias correction approach used in this work is the so-called change factor method (Diaz-Nieto and Wilby, 2005; Hay et al., 2000), and was applied for 30-year series centered over the years 2020, 2050 and 2080. In essence, this method modifies the observed historical time series by adding the difference between the future and actual climate as simulated by a GCM. These perturbation factors are computed for each month at each time period (2020, 2050 and 2080). This approach is applied for temperature (minimum and maximum) and precipitation data. Monthly variables from GCMs are used to modify the daily time series needed for hydrological modeling. Eqs. (1) and (2) show how this method is applied mathematically for minimal and maximal temperature Eq. (1) and precipitation Eq. (2). Indices are defined in the notation section.

$$T_{fut,j,h} = T_{obs,j} + (\overline{T}_{fut,m,h} - \overline{T}_{cont,m}) \quad (1)$$

$$P_{fut,j,h} = P_{obs,j} \times (\overline{P}_{fut,m,h}/\overline{P}_{cont,m}) \quad (2)$$

A region around the basin was defined to incorporate at least three grid points for each GCM. This common region allows similar averages to be defined for each GCM despite their distinct computational grids. Fig. 4 shows the common region superimposed on the computational grid of the five chosen GCMs.

An area-based weighting scheme for each grid is used to average monthly delta values for the basin. Eqs. (1) and (2) can be modified to take into account the weight of each grid point for all computational grids, to yield Eqs. (3) and (4). Indices correspond to all grid points within the common region defined around the basin.

$$T_{fut,j,h} = T_{obs,j} + [\omega_1(\overline{T}_{fut,m,h} - \overline{T}_{cont,m})_1 + \omega_2(\overline{T}_{fut,m,h} - \overline{T}_{cont,m})_2 + \cdots + \omega_n(\overline{T}_{fut,m,h} - \overline{T}_{cont,m})_n] \quad (3)$$

$$P_{fut,j,h} = P_{obs,j} \times [\omega_1(\overline{P}_{fut,m,h}/\overline{P}_{cont,m})_1 + \omega_2(\overline{P}_{fut,m,h}/\overline{P}_{cont,m})_2 + \cdots + \omega_n(\overline{P}_{fut,m,h}/\overline{P}_{cont,m})_n] \quad (4)$$

The monthly delta values obtained from Eqs. (3) and (4) are then applied to the daily observed historical data (precipitation and temperature).

Basin-averaged weather data

The hydrological model used in this study is a lumped model, which requires basin-averaged values of weather data. Minimum and maximum temperatures, as well as precipitation time series were averaged from observed data at all available stations. Delta minimum and maximum temperature values were directly added to basin-averaged series.

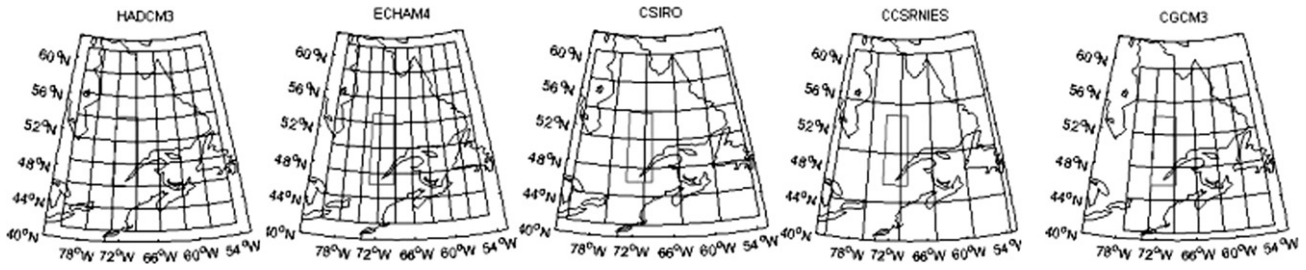

Figure 4 Interest zone with respect to the computational grid of the chosen GCMs.

Accounting for natural variability

The next step consisted in taking into account the uncertainty linked to natural variability. Natural variability was introduced into time series (for the control period and all climate change projections) using a stochastic weather generator. The WeaGets weather generator (Caron, 2005) was used. It is a Richardson (1981) type weather generator that uses a third-order Markov chain for daily precipitation occurrence and an exponential distribution function for quantity. An autoregressive process is used to generate minimum and maximum temperatures, based on whether a day is dry or wet. The weather generator allows the production of infinite-length time series with the same statistical properties as those of the original series. Once entered in the hydrological model, these long time series allow the natural climate variability to be assessed, and thus takes into account the uncertainty associated with just a single trace of the climate.

For each climate change scenario (and also for the observed historical time series) 30 series of 30 years were generated, giving a total of 900 years of daily synthetic climate data. It is important to note that these 900 years do not represent 900 consecutive years of evolving climate, but 900 years of climate with the same statistics as the 30-year series from which they were generated. Stationarity is an underlying assumption for each 30-year series. To sum it all up, eleven 900-year time series of daily minimum temperature, maximum temperature and precipitation were generated (2 GHGES for each of the 5 GCMs, as well as for the control period data).

Results

Seasonal change

Since the basin hydrology is closely linked to seasons, data analysis is performed on a seasonal basis. Projected precipitation and temperature change scatter plots are presented in Fig. 5 for all climate projections and chosen time slices (2020, 2050, 2080).

Fig. 5 indicates that for the chosen basin, all projections suggest a temperature increase for all chosen horizons. This increase varies from 1 to 4 °C in 2020 all the way to between 4 and 14 °C in 2080, depending on the season, GHGES and GCM. At each horizon, the temperature increase is largest in the winter (DJF) and smallest in the summer (JJA). It should also be noted that inter-model variability is largest

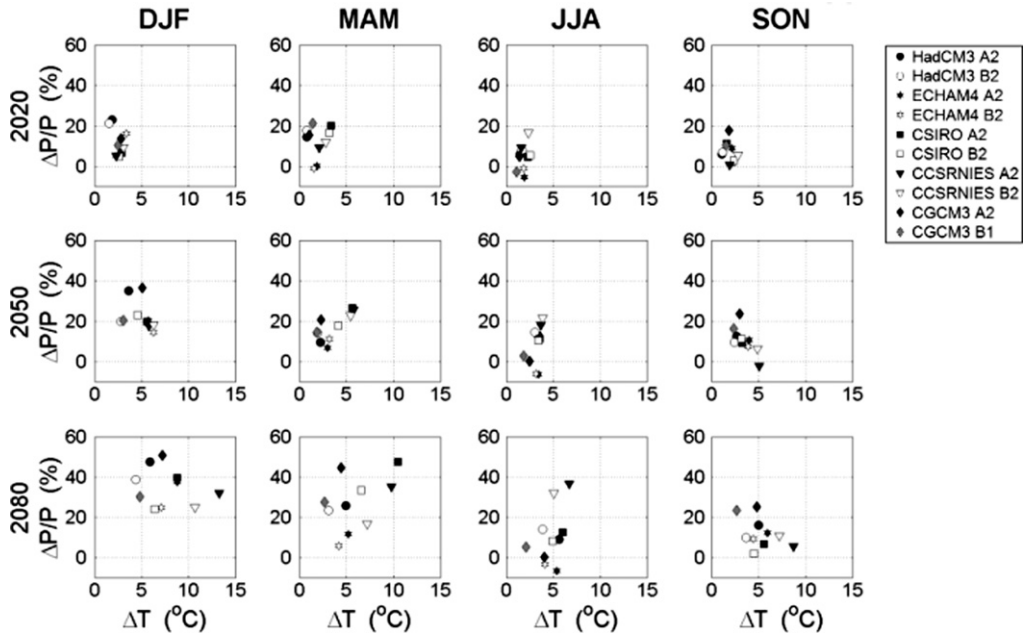

Figure 5 Scatter plots of temperature and precipitation seasonal changes for all combinations of GCM and GHGES, at the 2020, 2050 and 2080 time horizons.

in the winter (DJF) and spring (MAM) seasons. This is characterized by a larger dispersion on the scatter plots.

For precipitation, the GHGES and GCMs projections suggest an increasing trend by as much as 20% for 2020 and 55% for 2080. However, a few projections results in modest decreases in summer precipitation. For each time horizon, the maximum increase in precipitation is projected for the winter season (DJF).

For each season, inter-model variability increases with each time horizon, as shown by the increase in scatter in Fig. 5. In general, uncertainty linked with GCM is larger than that linked to GHGES. This is particularly obvious for the 2080 horizon. In other words, variability linked to GCM for a given scenario is larger than the variability linked to GHGES for that GCM.

Temperature variability

Fig. 6 presents the annual temperature cycle for all climate projections for the 2080 horizon. 900-year averages (thirty 30-year series) are shown in comparison to the synthetic data from the control period, which also averaged over 900 years.

It can also be seen from this figure that inter-model variability is greater than the variability induced by different emission scenarios. Temperature cycle graphs readily display the date on which average temperatures climb above — and descend below — freezing. Currently (bold line), these dates are April 15th and November 1st. Depending on the particular model and scenario, these dates could change to mid-March and mid-December, respectively by 2080. The freezing season could then be shortened by up to 2.5 months (from 5.5 to 3). This change would affect the hydrology of the basin by reducing snow accumulation over the winter and spring snowmelt, accordingly. The snowmelt period would also begin earlier.

Uncertainty of future average temperature and annual precipitation data

Fig. 7 shows the uncertainty envelope of climate data as a function of each combination of GCM and GHGES. In building this envelope, it was assume that each climate projection had an equal probability of occurrence. Using the results from the thirty 30-year simulations from the stochastic weather generator, empirical probability density functions (PDFs) of the basin's annual mean temperature and annual precipitation data were constructed. The PDFs display the range of possible values for each variable and for each time horizon. The probability that each variable will be below a certain value is equal to the area under the curve to the left of this given value. The total area under each PDF is equal to 1. For example, for annual precipitation data representatives of the control period (bold black line in all three graphs of the second row), expected values are between 650 and 1200 mm. The median is 964 mm (there is a 50% probability of annual precipitation being greater or smaller than 964 mm) and the mode (most frequent value) is 985 mm. While each of the individual PDFs in Fig. 7 displays the natural variability inherent in each climate projection (as modelled with the stochastic weather generator), the bold black dotted line is the PDF which includes all uncertainties, incorporating natural variability with GCM and GHGES variability.

Fig. 7 indicates that for both variables, uncertainty increases with time. PDFs also show that while all GCMs propose an annual increase in both temperature and precipitation for all projections, the magnitude of this

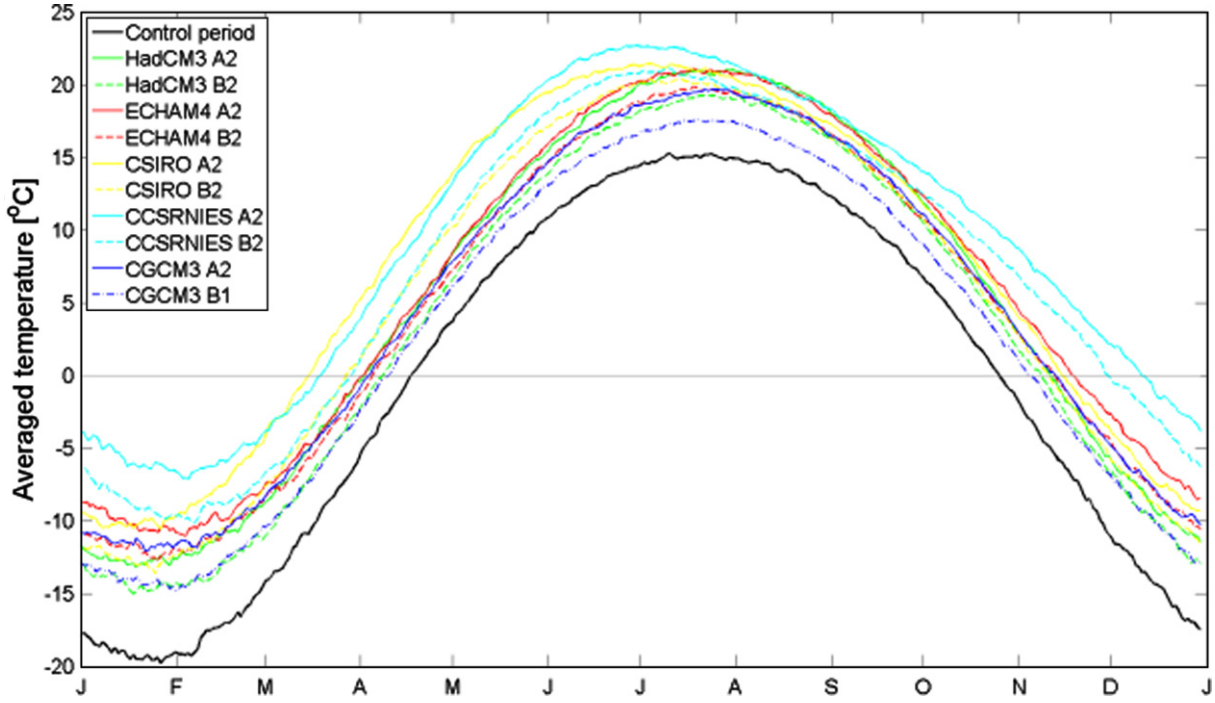

Figure 6 Averaged annual temperature cycle for all climate projections for the 2080 horizon, and for the 1961—1990 control period for the Chute-du-Diable watershed.

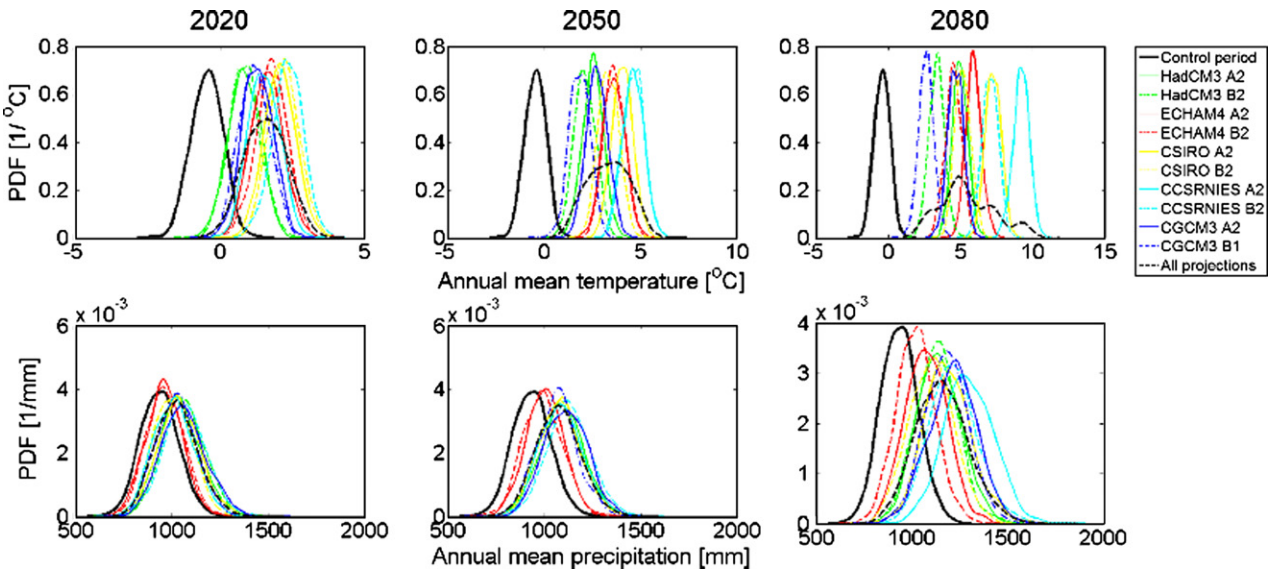

Figure 7 Probability density functions of annual mean temperature and annual precipitation data for all climate projections, and for the 1961—1990 control period. PDFs are presented for the 2020, 2050 and 2080 time horizons.

increase varies greatly from one GCM to the next. More precisely, climate projections from HadCM3 and CGCM3 show the smallest temperature increases, of about 0.5 and 3.5 °C for the 2020 and 2080 horizons, while the CCSRNIES and CSIRO models are at the other end of the spectrum, with increases of 2 and 8.5 °C for the same horizons. The middle-ground model is ECHAM4, with projected increases of 1.5 and 5.5 °C for the 2020 and 2080 horizons.

The GCMs behave differently for annual precipitation. ECHAM4 suggests the smallest annual precipitation increase, from less than 10 mm in 2020 to about 100 mm in 2080, and CCSRNIES proposes the largest increase, all the way up to 400 mm in 2080. The other 3 GCMs (HadCM3, CGCM3 and CSIRO) yield similar results, with increases ranging from 100 mm in 2020 to 200 mm in 2080.

The PDFs show that future average temperatures projected by GCMs will be fully distinct of the current natural variability by year 2050. This means that a cold year in the 2050 climate will be hotter than the current hottest year on record. This is not the case for precipitation, as can be seen from the overlaps between future climate PDFs and the one for the control period. This means that while the future is projected to become wetter over the basin, dry years will fall within the range of current observed values. By 2080, a very dry year would be one with precipitations close to the current mean of 962 mm.

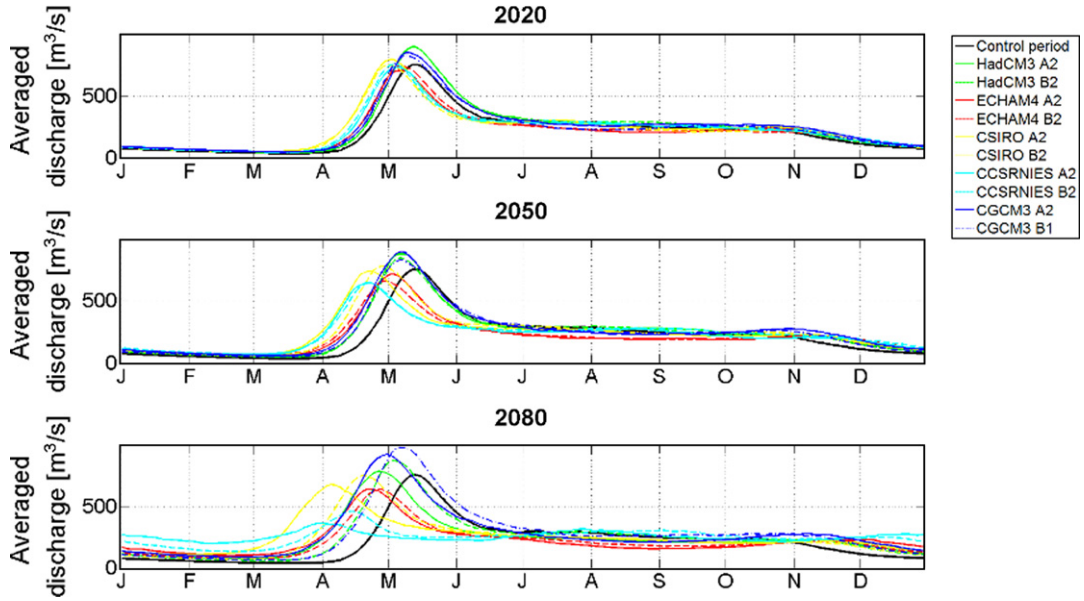

Figure 8 Average hydrographs for all climate projections, and for the 1961—1990 control period. Results are for the 2020, 2050 and 2080 time horizons.

Fig. 7 also shows that annual inter-model variability increases with time, for both precipitation and temperature. For precipitation, the within-model variability increases with time, as shown by PDFs that are flatter. This means that the variance in annual precipitation increases with time, indicating greater year-to-year variability.

Changes in annual variability are the result of the bias correction method which is applied on a monthly basis. Accordingly, variability is preserved at the monthly scale. However, with more distant time horizons, monthly correction factors increase and display more seasonal variability. This results in an increase in annual variability, which results in flatter PDFs.

Hydrologic impacts of climate change

Average hydrographs

Average hydrographs for each combination of GCMs and GHGES are presented in Fig. 8 for the three chosen time horizons. The averaged hydrographs are computed using 900 years of data from the stochastic weather generator (thirty 30-year time series). The bold line represents 900 years of the control period (1961—1990). In this figure as well as in those that follow, the control period will be represented by modelled data, and not real observed data. This is done to ensure that the slight bias observed in HSAMI simulations is taken into account when comparing the future to the control period.

Fig. 8 indicates that there is a general increase in winter flows (November—April) projected by all GCMs, and for all three time horizons. A decrease in summer flows (June—October) is observed in most cases for the 2020 and 2050 horizons, and in all cases, but for CCSRNIES A2, in 2080. Peak discharge is observed sooner in all cases and horizons. The lag varies from a few days in 2020 all the way to 6 weeks in 2080, depending on the GCM and GHGES selected. Results do not converge in the case of peak discharge magnitude. CGCM3 and HadCM3 propose an increase in peak discharge for all projections and time horizons while the other three GCMs project either the status quo or a decrease in peak discharge. In particular, the CCSRNIES model suggest a severe decrease in peak discharge (especially for the A2 scenario), with a very early occurrence, as well as a high average discharge over the winter.

Annual and seasonal inflows

Total annual and seasonal inflows are presented in Fig. 9 for all climate change projections as well as for the control period. Results are presented in % of the simulated control period for all three time horizons. As mentioned before, a comparison is done with modeled inflows, and not with observed ones, in order to avoid any bias due to the hydrological model. As such, reconstructed inflows for the control period are always at 100%.

For annual inflows, the only simulations that project a decrease come from the ECHAM4 model. This decrease is projected for all three time horizons and varies from 1% to 7%, depending on the particular scenario and time horizon. For the other models, increases varying from 1% to 20% are projected. In addition to changes in mean annual inflows, a seasonal redistribution of inflows is also observed. At the seasonal scale, the largest increases are in winter (DJF), and the smallest in summer (JJA). The largest increase (290%) results from CCSRNIES A2 in 2080, and the largest decrease (30%) is projected by ECHAM4 A2, also in 2080.

All observed changes in annual mean inflows are statistically significant (5% level) for all projections and all horizons, with the exception of ECHAM4 A2 in 2050 and ECHAM4 B2 in 2020 and 2080. Changes in variance are also

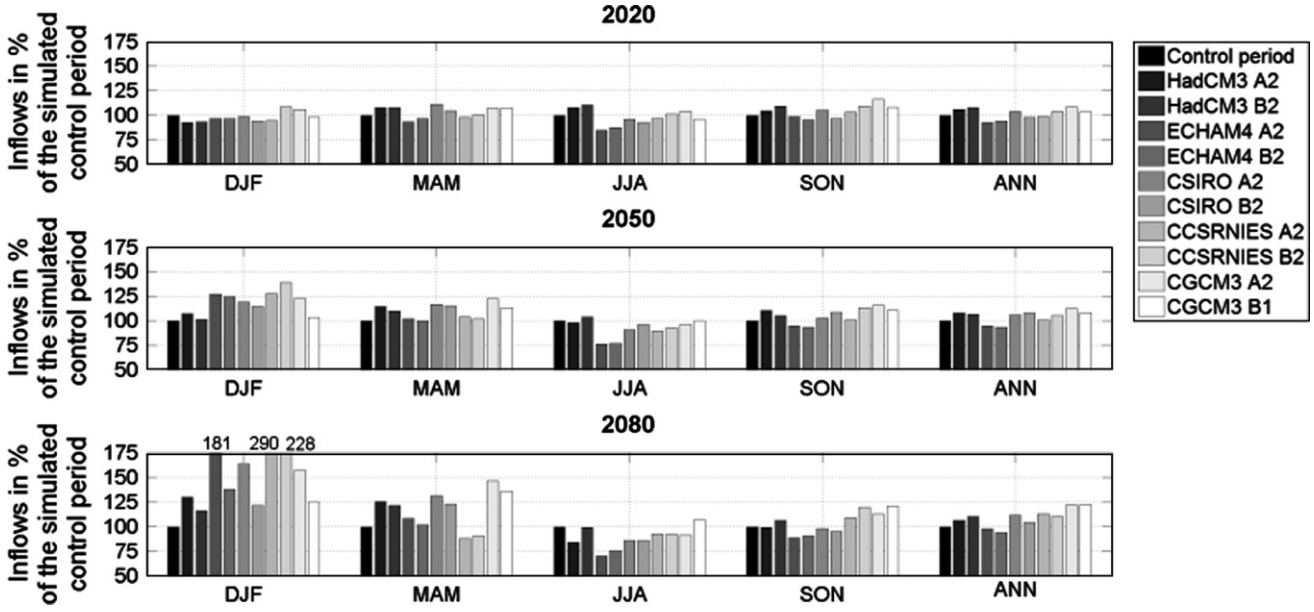

Figure 9 Total seasonal and annual inflows for all climate projections and for the control period, in percentage of the inflows of the control period. Results are for the 2020, 2050 and 2080 time horizons.

significant (5% level) with the exception of ECHAM4 A2 and B2 for each horizon and CSIRO A2 in 2020. At the seasonal scale, changes in mean and variance are significant (1% level) for all seasons, projections and time horizons. Standard *t*-test and *F*-test were used as seasonal and annual inflows followed a normal distribution.

Peak discharge

The snowmelt peak discharge is analyzed based on magnitude and time of occurrence criteria. Figs. 10 and 11 present averages of these criteria for all climate change projections and time horizons. This data can also be ex-

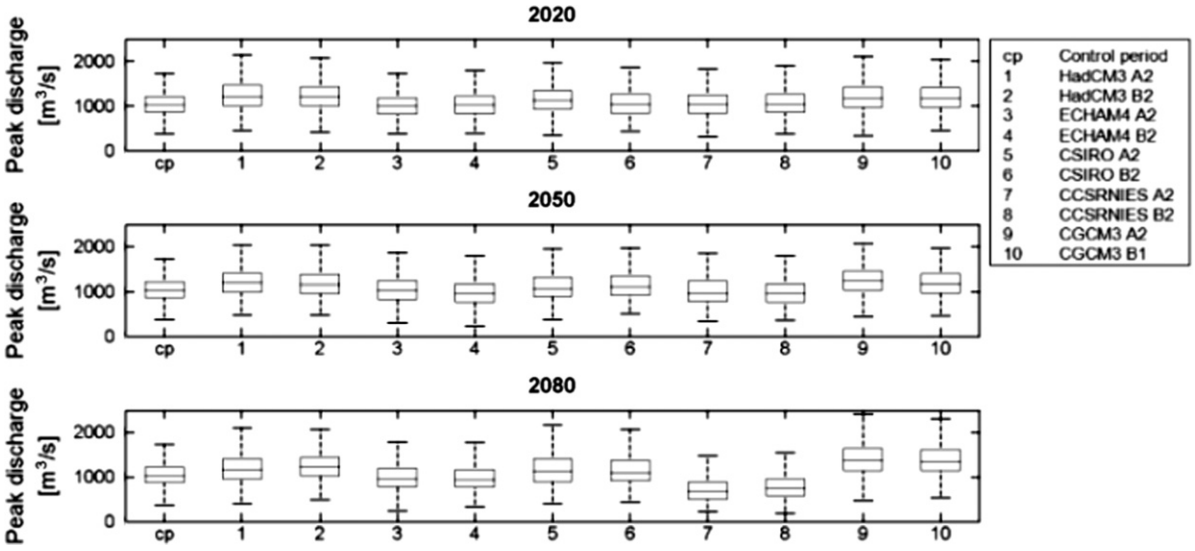

Figure 10 Snowmelt peak discharge for all climate projections, and for the 1961—1990 control period (cp). Results are for the Chute-du-Diable watershed at the 2020, 2050 and 2080 time horizons.

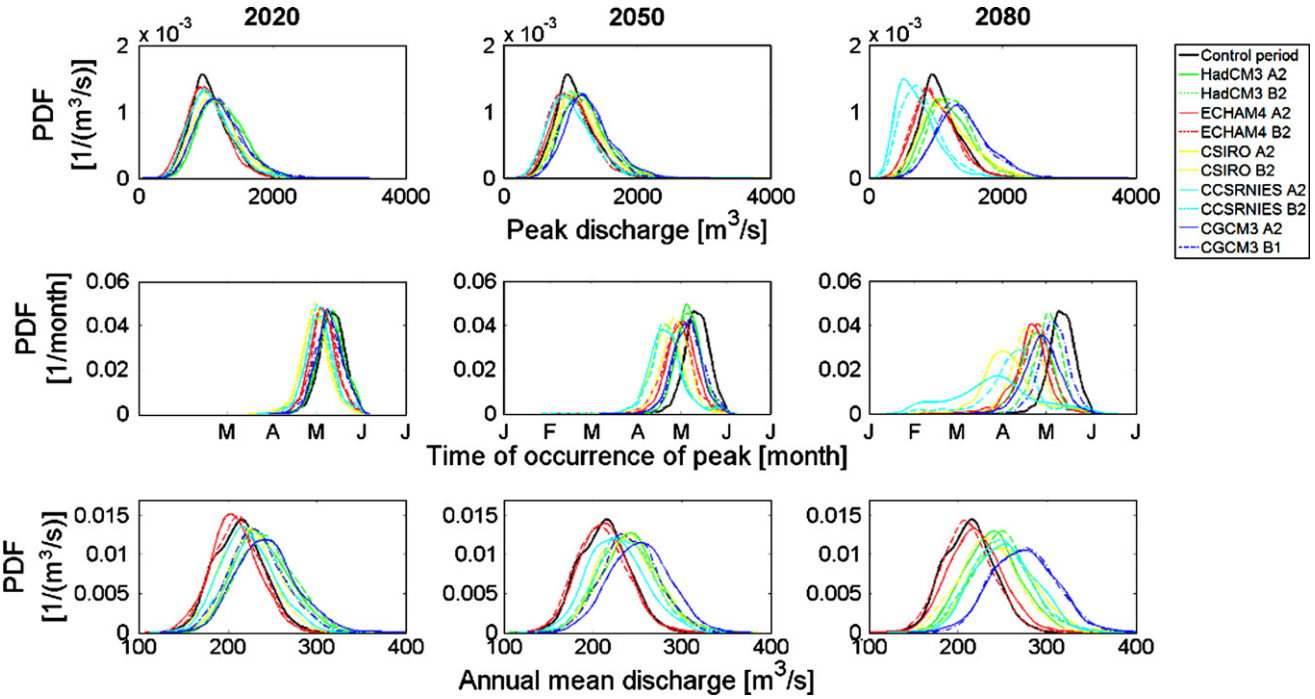

Figure 11 Probability density functions of peak discharge (top row), time of occurrence of peak (middle row) and annual mean discharge (bottom row), for all climate projections, and for the 1961—1990 control period. PDFs are presented for the 2020, 2050 and 2080 time horizons.

Table 2 Averaged time of occurrence of peak discharge for all climate projections, and for the 1961—1990 control period

Control period	2020	2050	2080
	11 May		
HadCM3 A2	10 May (1)	5 May (6)	23 April (18)
HadCM3 B2	10 May (1)	5 May (6)	1 May (10)
ECHAM4 A2	5 May (6)	30 April (11)	19 April (22)
ECHAM4 B2	6 May (5)	28 April (13)	23 April (18)
CSIRO A2	30 April (11)	21 April (20)	4 April (37)
CSIRO B2	30 April (11)	26 April (15)	18 April (23)
CCSRNIES A2	3 May (8)	20 April (21)	26 March (46)
CCSRNIES B2	2 May (9)	21 April (20)	8 April (33)
CGCM3 A2	9 May (2)	4 May (7)	27 April (14)
CGCM3 B1	9 May (2)	6 May (5)	5 May (6)

The number in parenthesis indicates how earlier the peak discharge is (in days) when compared to the control period. Results are for the 2020, 2050 and 2080 time horizons.

tracted from Fig. 8, but is more easily visualized in Figs. 10 and 11.

Fig. 10 presents peak discharge values. By 2020, HadCM3, under scenarios A2 and B2, suggest a 12% (median) increase in peak discharge, whereas ECHAM4 under the A2 scenario, propose a 2% (median) decrease. By 2080, the CCSRNIES model under the A2 scenario propose the largest decrease (40%) whereas the largest increase at 25% is projected by CGCM3 A2. All models predict an increased variability compared to the control period.

The combined effects of temperature and precipitation changes influence peak discharge differently depending on the GCM. Models that predict the highest increases in winter and spring temperature (ECHAM4 and CCSRNIES) forecast a reduced peak discharge. Liquid winter precipitation rapidly contributes to runoff instead of being stocked in the snow cover, thus reducing the potential of a high peak discharge. Higher winter temperatures also contribute to episodic melting of the snow cover throughout the winter and early spring. The models HadCM3, CSIRO and CGCM3, which predict smaller increases in winter temperatures, result in increases in peak discharge. For these two models, increases in winter temperatures are not sufficient to offset the precipitation increase. In other words, more abundant winter precipitation results in a thicker spring snowpack, despite the increased likelihood of winter rainfall and episodic snowmelt.

For the time of occurrence of peak discharge, Table 2 indicates that models predict either no change or an earlier peak by a maximum of 12 days (from May 11 to April 30 for CSIRO A2) in 2020. The 2050 and 2080 time horizons display much wider variabilities between projections with a time of occurrence as early as March 26 (CCSRNIES A2) and as late as May 5th (CGCM3 B1).

Uncertainty of hydrologic variables

Probability density functions (PDFs) are shown in Fig. 11 for the peak discharge (top row), the time of occurrence of peak discharge (middle row) and for the mean discharge (last row). The PDFs allow the uncertainty of each variable to be better quantified.

Results show that uncertainty increases with time, as PDFs become flatter and inter-model variability becomes larger. A greater variance of the hydrologic variables is also observed as PDFs become generally flatter with time.

There is no consensus among models on changes in the peak monthly discharge, with ECHAM4 projecting increases and CCSNRIES projecting decreases.

For the time of occurrence, all projections suggest an early spring flood but 2 models predict particularly important changes in 2080. The spring flood occurs earlier by about 6 weeks with CSIRO A2, as its PDF is shifted to the left. Scenario CCSRNIES A2 also suggests a similar early flood, but its uncertainty is much larger than that of the other models, as shown by a very flat PDF.

For the annual mean discharge, there is less variability as most models project a small to moderate increase. Two exceptions are ECHAM4 A2, which suggest a decrease in mean discharge and CGCM3 A2, which propose a relatively large increase in mean discharge. In the latter case, half of the years produce a mean discharge larger than the maximum mean discharge currently observed.

Discussion

The analysis of the potential impacts of climate change on the Chute-du-Diable watershed first reveals that all projections show a temperature increase over the basin for all seasons. Projected changes in precipitation are not univocal, and vary depending on the GCM, GHGES, time horizon, and on the season. Hydrologic changes result from a combination of these variables. Most hydrologic simulations suggest an increase in annual mean discharge, a decrease in peak discharge as well as an early spring snowmelt. There is however much variability between models and scenarios, and this variability increases when an attempt is made to project events for a more distant future. For this reason, any climate change impact study based on only one GCM or GHGES should be accompanied by a cautionary warning. It has been suggested that the use of two carefully chosen climate projections (dry/hot and wet/cold projections as an example) may be sufficient (e.g. (Brekke et al., 2004;

Singh et al., 2006)). However, the process by which climate projections become hydrologic variables is not a linear one, and notable seasonal variability may render the choice of projections incorrect. A good example is the CCSRNIES model. While most other models generate mean hydrographs that are similar in shape (Fig. 8), those for the CCSRNIES model are markedly different, particularly in the winter and spring seasons. Fig. 5 indicates that CCSRNIES is a 'very warm' and 'moderately wet' model over the winter and has its tendency reversed over the summer to 'moderately warm' and 'very wet'. On the scatter plots, the model is always at the outer edge of the clusters. The warm winters projected by the model drastically reduce snow accumulation and almost remove the spring peak discharge. Winter rainfalls and increased temperatures both result in higher winter runoff, and a reduced peak discharge. Another example of potential hydrological impact is outlined by the ECHAM4 model. Fig. 9 shows that ECHAM4 is the only model that predicts decreasing mean annual inflows. ECHAM4 is a 'moderately warm' model that forecasts mild increases in annual precipitation (moderate increases or decreases on a seasonal basis). Even if annual precipitation is on the rise, annual inflows nevertheless decrease due to rising evapotranspiration resulting in a net water loss.

There are several limits to the approach presented in this paper, and uncertainties that have not been taken into account, the most important one probably being the downscaling method. Like all downscaling approaches, the change factor method has its advantages and limitations. The main problem of the method is that it does not modify the temporal and spatial structure of precipitation and temperature data (Diaz-Nieto and Wilby, 2005; Fowler et al., 2005). For example, the time series of precipitation occurrence will remain unchanged. The change factor method will also not modify the variance of temperature data. In some applications, it may be just as important to evaluate changes in the variance of future climate variables and not only changes in the means (Semenov et al., 1998). The weather generator was used to partly offset these downsides by allowing natural variability to be built into the analysis. Through the use of distribution functions, a change in mean precipitation will result in a change in precipitation variance. Coupled with a stochastic weather generator, the remaining main weakness of the change factor method lies in the unchanged precipitation occurrence structure. While the method will yield precipitation occurrence time series that vary from one year to the next, the transition probabilities from a dry day to a rainy one (and from rainy to dry) remain the same. This means that the approach proposed in this paper would clearly be inadequate for a study on dry spells or water shortages in the dry season. However, for a study focusing on a basin where the most important hydrologic features are linked to snow accumulation and snowmelt, this weakness is not problematic. Diaz-Nieto and Wilby (2005) recommend the change factor method for a broad-brush high-level assessment of climate change impacts and suggest more complex statistical downscaling techniques for the investigation of more subtle changes in the temporal sequencing and persistence of daily events.

On the other hand, the change factor method presents several advantages. It is a simple method to implement, and only requires information from GCMs at the monthly time scale. The change factor method readily takes this monthly information and brings it to the daily-scale required for hydrological modelling. Most other statistical downscaling methods need data from GCMs at the daily time scale. Daily-scale data from GCMs is considered less accurate by many (Huth et al., 2001; Palutikof et al., 1997). Bias correction and variance adjustment is needed to obtain merely adequate results, whereas with the change factor method, bias correction is implicitly built into the approach. Moreover, daily-scale GCM data is not available for many GCMs and GHGES. As such, the approach presented in this paper would not be feasible. The same can be said of dynamic downscaling methods (higher-resolution climate models). While variables at the daily time scale from higher-resolution climate models are considered more reliable, such data is not easily available. Additionally, most higher-resolution climate models are not run over a global grid, and must use boundary conditions from GCMs. As such, they retain part of the bias of the GCM used to drive the simulation. For the work presented in this paper, changes in precipitation and temperature means are the key variables that need to be estimated and the change factor method is appropriate for this purpose.

The use of only two greenhouse gases emissions scenarios also constitutes a limitation for this study. In their special report on emissions scenarios, the IPCC (Nakicenovic et al., 2000) presented 40 scenarios under four large families (A1, A2, B1, B2). However, the computing cost of running all scenarios in GCMs is prohibitive. As such, the IPCC (Nakicenovic et al., 2000) recommends the use of the A2 (high emissions) and B2 (medium-low emissions) for inter-comparison studies. These two scenarios are the only ones that were common to all of the selected GCMs. The fact that inter-model variability is greater than inter-scenario variability also supports the choice of those two scenarios as being adequate.

Another limitation to the approach presented in this paper is linked to hydrologic model calibration. The approach implicitly assumes that the calibration will hold in the future. Even though, calibration and validation were performed based on the more recent and hotter years on record. Following suggestions made by Dietterick et al., 1999 a careful examination of the performance of the hydrologic model over the existing record did not reveal any notable differences in performance between colder/wetter years and hotter/dryer years. This is an indication that the model may perform well for a future climate.

The use of a more physically-based model may help reduce the uncertainty linked to calibration. However, Jones et al., 2006 have shown that a 10-parameter lumped model did perform just as well as a more physically realistic but complex spatially distributed model, with respect to annual inflows in a climate change study. A multi-model approach (Georgakakos et al., 2004) may be the best approach to better understand the uncertainty linked to the choice of models. However, it is expected that the large variability induced by the different GCMs, as shown in this paper, will dwarf the one induced by the choice of one hydrological model or specific model calibration over another. That should (and currently is) be investigated in future work.

Finally, it would be interesting to apply the methodology presented in this work to other basins in order to explore

the uncertainty linked to physical characteristics, geographical location and climate zones.

Conclusion

The objective of this work was to estimate the uncertainty respecting the impact of climate change on the hydrology of a Nordic Watershed. This work is the first step in a project that looks at adaptation measures for the Peribonka River basin. Future work will build on the results of this paper, and will look at the impacts of climate change on hydropower production and management practice over the basin.

This work uses a multi-model, multi-projection approach to generate probability distribution functions of future hydrologic variables. This probabilistic approach helps to better define the uncertainty linked to future climate. Results indicate that a large uncertainty exists in all the projected future hydrologic variables. Of all the potential sources of uncertainty, the one induced by the choice of a general circulation model (GCM) is the largest. As such, any impact study based on data from a single GCM should be interpreted with great care. The probability distributions of future hydrologic variables allow the likelihood of future impacts to be estimated. Based on these, it is reasonable to say that the hydrologic behaviour of the Chute-du-Diable basin would be progressively modified over the next century.

While it impossible to predict future flows, one thing that can be done, and should be done, is to include the increased uncertainty of future hydrologic variables into design and management practices.

Acknowledgement

This paper is part of a larger project funded by the Ouranos Consortium on Regional Climatology and Adaptation to Climate Change (www.ouranos.ca) and the Natural Science and Engineering Research Council of Canada (NSERC). In particular, the authors would like to thank Diane Chaumont of Ouranos, for her help in preparing the climate change projections.

References

Bisson, J.L., Roberge, F. (1983). Prévisions des apports naturels: Expérience d'Hydro-Québec. Paper presented at the Workshop on flow predictions, Toronto.

Boer, George G., 2004. Long time-scale potential predictability in an ensemble of coupled climate models. Climate Dynamics 23, 29–44.

Brekke, Levi. D., Miller, Norman L., Bashford, Kathy E., Quinn, Nigel W.T., Dracup, John A., 2004. Climate change impacts uncertainty for water resources in the San Joaquin River Basin, California. Journal of the American Water Resources Association 40 (1), 149–164.

Caron, Annie. (2005). Étalonnage et validation d'un générateur de climat dans le contexte des changements climatiques. École de technologie supérieure, Montréal.

Christensen, Niklas S., Wood, Andrew W., Voisin, Nathalie, Lettenmaier, Dennis P., Palmer, Richard N., 2004. The effects of climate change on the hydrology and water resources of the Colorado river basin. Climatic Change 62, 337–363.

Diaz-Nieto, Jacqueline, Wilby, Robert L., 2005. A comparison of statistical downscaling and climate change factor methods: impacts on low-flows in the river Thames United Kingdom. Climatic Change 69, 245–268.

Dietterick, Brian C., Lynch, James A., Corbett, Edward S., 1999. A calibration procedure using topmodel to determine suitability for evaluating potential climate change effects on water yield. Journal of the American Water Resources Association 35 (2), 457–468.

Duan, Q., 2003. Calibration of watershed models. In Duan, Q., Gupta, H., Sorooshian A.N. (Eds.), Water science and application, vol. 6, Washington D.C., pp. 89–104.

Environement Canada, 2004. Menaces pour la disponibilité de l'eau au Canada. Burlington (Ontario): Institut National de Recherche Scientifique, 148 p.

Fortin, Vincent, 2000. Le modèle météo-apport HSAMI: historique, théorie et application. Varennes: Institut de Recherche d'Hydro-Québec, 68 p.

Fowler, H.J., Kilsby, C.G., O'Connel, P.E., Burton, A., 2005. A weather-type conditioned multi-site stochastic rainfall model for the generation of climatic variability and change. Journal of Hydrology 38, 50–66.

Georgakakos, Konstantine P., Seo, Dong-Jun, Gupta, Hoshin, Schaake, John, Butts, Michael B., 2004. Towards the characterization of streamflow simulation uncertainty throught multimodel ensembles. Journal of Hydrology 298, 222–241.

Hay, L.E., Wilby, Robert L., Leavesly, H.H., 2000. Comparison of delta change and downscaled GCM scenarios for three mountainous basins in the United States. Journal of the American Water Resources Association 36 (2), 387–397.

Huth, Radan, Kysely, Jan, Dubrovsky, Martin, 2001. Time structure of observed, GCM-simulated, downscaled, and stochastically generator daily temperature series. Journal of Climate 14 (20), 4047–4061.

IPCC, Intergovernmental Panel on Climate Change, 2001. Climate change 2001: The Scientific Basis. Wembley, Royaume-Unis, 882 p.

Jones, Roger N., Chiew, Francis H.S., Boughton, Walter C., Zhang, Lu, 2006. Estimating the sensitivity of mean annual runoff to climate change using selected hydrological models. Advances in Water Resources 29 (10), 1419–1429.

Maurer, Edwin P., 2007. Uncertainty in hydrologic impacts of climate change in the Sierra Nevada, California, under two emissions scenarios. Climatic Change 82, 309–325.

Merritt, Wendy S., Alila, Younes, Barton, Mark, Taylor, Bill, Cohen, Stewart, Neilsen, Denise, 2006. Hydrologic response to scenarios change in sub watersheds of the Okanagan basin, British Columbia. Journal of Hydrology 326, 79–108.

Muzik, Ivan, 2001. Sensitivity of hydrologic systems to climate change. Canadian Water Resources Journal 26 (2), 233–253.

Nakicenovic, N., J. Alcamo, G. Davis, B. de Vries, J. Fenhann, S. Gaffin, K. Gregory, A. Grübler, T.Y. Jung, T. Kram, E.L. La Rovere, L. Michaelis, S. Mori, T. Morita, W. Pepper, H. Pitcher, L. Price, K. Raihi, A. Roehrl, H-H. Rogner, A. Sankovski, M. Schlesinger, P. Shukla, S. Smith, R. Swart, S. van Rooijen, N. Victor, Dadi, Z. (2000). IPCC Special Report on Emissions Scenarios. United Kingdom and New York, NY, USA, 599 p.

Ouranos, 2004. S'adapter aux changements climatiques. Montréal: Consortium sur la Climatologie régionale et l'adaptation aux Changements Climatiques, 83.

Palutikof, J.P., Winkler, J.A., Goodess, C.M., Andresen, J.A., 1997. The simulation of daily temperature time series from GCM Output. Part 1: comparison of model data with observations. Journal of Climate 10, 2497–2513.

Prudhomme, Christel, Jakob, Dörte, Svensson, Cecilia, 2003. Uncertainty and climate change impact on the flood regime of small UK catchments. Journal of Hydrology 277, 1–23.

Regonda, Satish Kumar, Rajagopalan, Balaji, Clark, Martyn, Pitlick, John, 2005. Seasonal cycle shifts in hydroclimatology over the western United States. Journal of Climate 18 (2), 372—384.

Richardson, Clarence W., 1981. Stochastic simulation of daily precipitation, temperature, and solar radiation. Water Resources Research 17 (1), 182—190.

Risbey, James S., Entekhabi, Dara, 1996. Observed Sacremento Basin streamflow response to precipitation and temperature changes and its relevance to climate impact studies. Journal of Hydrology 184, 209—223.

Roy, Luc, Brissette, François, Leconte, Robert, Marche, Claude, 2001. The impact of climate change on seasonal floods of a southern Quebec River Basin. Hydrological Processes 15, 3167—3179.

Semenov, Mikhail A., Brooks, Roger J., Barrow, Elaine M., Richardson, Clarence W., 1998. Comparison of the WGEN and LARS-WG stochastic weather generators for diverse climates. Climate Research 10, 95—107.

Singh, Pratap, Arora, Manohar, Goel, N.K., 2006. Effect of climate change on runoff of a glacierized himalayan basin. Hydrological Processes 20, 1979—1992.

Srikanthan, R., McMahon, T.A., 2001. Stochastic generation of annual, monthly and daily climate data: a review. Hydrology and Earth Systems Sciences 5 (4), 653—670.

Vicuna, Sebastian, Maurer, Edwin P., Joyce, Brian, Dracup, John A., Purkey, David, 2007. The sensitivity of California water resources to climate change scenarios. Journal of the American Water Resources Association 43 (2), 482—498.

Whitfield, Paul H., Cannon, Alex J., 2000. Recent variation in climate and hydrology in Canada. Canadian Water Resources Journal 25 (1), 19—65.

Xu, Chong-Yu, Singh, V.P., 2004. Review on regional water resources assessment models under stationary and changing climate. Water Resources Management 18, 591—612.